morphologic evaluation of the phenotype of valvular interstitial cells in dogs with myxomatous degeneration of the mitral valve. *Am J Vet Res* 2005;66:1408–1414.
9. Disatian S, Ehrhart EJ III, Zimmerman S, et al. Interstitial cells from dogs with naturally occurring myxomatous mitral valve disease undergo phenotype transformation. *J Heart Valve Dis* 2008;17:402–411.
10. Han RI, Black A, Culshaw GJ, et al. Distribution of myofibroblasts, smooth muscle-like cells, macrophages, and mast cells in mitral valve leaflets of dogs with myxomatous mitral valve disease. *Am J Vet Res* 2008;69:763–769.
11. Weber H, Webb ML, Serafino R, et al. Endothelin-1 and angiotensin-II stimulate delayed mitogenesis in cultured rat aortic smooth muscle cells: evidence for common signaling mechanisms. *Mol Endocrinol* 1994;8:148–158.
12. Rizvi MA, Katwa L, Spadone DP, et al. The effects of endothelin-1 on collagen type I and type III synthesis in cultured porcine coronary artery vascular smooth muscle cells. *J Mol Cell Cardiol* 1996;28:243–252.
13. Mow T, Pedersen HD. Increased endothelin-receptor density in myxomatous canine mitral valve leaflets. *J Cardiovasc Pharmacol* 1999;34:254–260.
14. Olsen LH, Mortensen K, Martinussen T, et al. Increased NADPH-diaphorase activity in canine myxomatous mitral valve leaflets. *J Comp Pathol* 2003;129:120–130.
15. Aupperle H, Thielebein J, Kiefer B, et al. An immunohistochemical study of the role of matrix metalloproteinases and their tissue inhibitors in chronic mitral valvular disease (valvular endocardiosis) in dogs. *Vet J* 2009;180:88–94.
16. Aupperle H, Marz I, Thielebein J, et al. Expression of transforming growth factor-beta1, -beta2 and -beta3 in normal and diseased canine mitral valves. *J Comp Pathol* 2008;139:97–107.
17. Mahimkar R, Nguyen A, Mann M, et al. Cardiac transgenic matrix metalloproteinase-2 expression induces myxomatous valve degeneration: a potential model of mitral valve prolapse disease. *Cardiovasc Pathol* 2009;18:253–261.
18. Ng CM, Cheng A, Myers LA, et al. TGF-beta-dependent pathogenesis of mitral valve prolapse in a mouse model of Marfan syndrome. *J Clin Invest* 2004;114:1586–1592.
19. Dreger SA, Taylor PM, Allen SP, et al. Profile and localization of matrix metalloproteinases (MMPs) and their tissue inhibitors (TIMPs) in human heart valves. *J Heart Valve Dis* 2002;11:875–880.
20. Annes J, Munger JS, Rifkin DB. Making sense of latent TGFbeta activation. *J Cell Sci* 2003;116:217–224.
21. Kaartinen V, Warburton D. Fibrillin controls TGF-beta activation. *Nat Genet* 2003;33:331–332.
22. Charbonneau NL, Ono RN, Corson GM, et al. Fine tuning of growth factor signals depends on fibrillin microfibril networks. *Birth Defects Res C Embryo Today* 2004;72:37–50.
23. Ramirez F, Sakai L, Dietz H, et al. Fibrillin microfibrils: multipurpose extracellular networks in organismal physiology. *Physiol Genomics* 2004;19:151–154.
24. Rifkin DB. Latent transforming growth factor-beta (TGF-beta) binding proteins: orchestrators of TGF-beta availability. *J Biol Chem* 2005;280:7409–7412.
25. Togashi M, Tamura K, Nitta T, et al. Role of matrix metalloproteinases and their tissue inhibitor of metalloproteinases in myxomatous change of cardiac floppy valves. *Pathol Int* 2007;57:251–259.
26. Buchanan JW. Patent ductus arteriosus. *Semin Vet Med Surg (Small Anim)* 1994;9:168–176.
27. Buchanan JW, Bücheler J. Vertebral scale system to measure canine heart size in radiographs. *J Am Vet Med Assoc* 1995;206:194–199.
28. Pouchelon JL, Jamet N, Gouni V, et al. Effect of Benazepril on survival and cardiac events in dogs with asymptomatic mitral valve disease: a retrospective study of 141 cases. *J Vet Intern Med* 2008;22:905–914.
29. Whitney JC. Cardiovascular pathology. *J Small Anim Pract* 1967;8:459–465.
30. Pho M, Lee W, Watt DR, et al. Cofilin is a marker of myofibroblast differentiation in cells from porcine aortic cardiac valves. *Am J Physiol Heart Circ Physiol* 2008;294:1767–1778.
31. Tamura K, Fukuda Y, Ishizaki M, et al. Abnormalities in elastic fibers and other connective-tissue components of floppy mitral valve. *Am Heart J* 1995;129:1149–1158.
32. Mercado-Pimentel ME, Runyan RB. Multiple transforming growth factor-beta isoforms and receptors function during epithelial-mesenchymal cell transformation in the embryonic heart. *Cells Tissues Organs* 2007;185:146–156.
33. Norris RA, Potts JD, Yost MJ, et al. Periostin promotes a fibroblastic lineage pathway in atrioventricular valve progenitor cells. *Dev Dyn* 2009;238:1052–1063.
34. Pho M, Lee W, Watt DR, et al. Cofilin is a marker of myofibroblast differentiation in cells from porcine aortic cardiac valves. *Am J Physiol Heart Circ Physiol* 2008;294:H1767–H1778.
35. Neidlinger-Wilke C, Würtz K, Urban JP, et al. Regulation of gene expression in intervertebral disc cells by low and high hydrostatic pressure. *Eur Spine J* 2006;15(suppl 3):S372–S378.
36. Das RH, Jahr H, Verhaar JA, et al. In vitro expansion affects the response of chondrocytes to mechanical stimulation. *Osteoarthritis Cartilage* 2008;16:385–391.
37. Li XC, Zhuo JL. Intracellular ANG II directly induces in vitro transcription of TGF-beta1, MCP-1, and NHE-3 mRNAs in isolated rat renal cortical nuclei via activation of nuclear AT1a receptors. *Am J Physiol Cell Physiol* 2008;294:C1034–C1045.
38. Zhang N, Wu XY, Wu XP, et al. Relationship between age-related serum concentrations of TGF-beta1 and TGF-beta2 and those of osteoprotegerin and leptin in native Chinese women. *Clin Chim Acta* 2009;403:63–69.
39. Hering S, Isken F, Janott J, et al. Analysis of TGF-β3 gene expression and protein levels in human bone and serum. *Exp Clin Endocrinol Diabetes* 2001;109:107–115.
40. Bonnema DD, Webb CS, Pennington WR, et al. Effects of age on plasma matrix metalloproteinases (MMPs) and tissue inhibitor of metalloproteinases (TIMPs). *J Card Fail* 2007;13:530–540.

Pediatr Cardiol (2011) 32:1244–1248
DOI 10.1007/s00246-011-0078-6

CASE REPORT

A Case of Cor Triatriatum With an Abnormal P Wave: The Pacemaker Action From the Specialized Tissue in the Abnormal Septum

Yoshimichi Kudo · Mariko Kaneko · Makoto Nakazawa · Sachiko Tomita

Received: 14 April 2011 / Accepted: 20 July 2011 / Published online: 7 August 2011

Abstract A boy presented with an abnormal P wave shown on an electrocardiogram (ECG) checkup at school. An echocardiogram and contrast-enhanced computed tomography (CT) showed cor triatriatum with a slit-like opening between the accessory chamber and the left atrium located along the interatrial septum. The boy underwent open heart surgery for excision of the anomalous membrane, and a postoperative ECG showed normal P waves. The excised tissue was examined immnunohistopathologically using antihyperpolarization-activated cyclic nucleotide-gated potassium channel 4 (HCN4) antibody and other staining. The authors confirmed the existence of cells positive to HCN4, indicating that they were sinoatrial node cells or at least cells with electrical automaticity.

Keywords ECG checkup · HCN4 · Sinoatrial node cell

Electronic supplementary material The online version of this article (doi:10.1007/s00246-011-0078-6) contains supplementary material, which is available to authorized users.

Y. Kudo (✉) · M. Kaneko
Department of Pediatrics, Southern Tohoku Research Institute for Neuroscience, Southern Tohoku General Hospital, 7-115 Yatsuyamada, Koriyama, Fukushima 963-8563, Japan
e-mail: yoshimichi.kudo@mt.strins.or.jp

M. Nakazawa
Pediatric and Lifelong Congenital Cardiology Institute, Southern Tohoku Research Institute for Neuroscience, Southern Tohoku General Hospital, 7-115 Yatsuyamada, Koriyama, Fukushima 963-8563, Japan

S. Tomita
Department of Pediatric Cardiology, Tokyo Women's Medical University, Tokyo, Japan

Case Report

A 10-year-old boy who was totally asymptomatic and had no congenital heart disease in his family history presented with an abnormal P wave shown in on electrocardiogram (ECG) checkup. He had no abnormal physical findings. His ECG (Fig. 1a) showed large negative P waves in II, III, and aVF and negative P waves in V5 and V6. A chest x-ray was not remarkable, but a questionable double contour was observed, suggesting mild left atrial enlargement.

To exclude any anomalies associated with the abnormal P waves, we performed an echocardiographic examination, which showed an anomalous membrane in the left atrium separating it into two chambers. The one chamber received the pulmonary veins, and the other chamber had the mitral valve, thus leading to the diagnosis of cor triatriatum, classic type as defined in the Moss and Adams' textbook [3]. The opening between the left atrium and the accessory chamber was slit-like and located along the interatrial septum. Its long axis measured 7 mm (Fig. 2). No obvious deviation of the anomalous membrane toward the proper left atrium was observed, indicating that there was no significant hemodynamic obstruction due to the membrane at the time. However, all the pulmonary veins appeared to be somewhat dilated, indicating a subtle and mild pulmonary congestion.

A contrast-enhanced CT confirmed the presence of the opening resembling a slit adjacent to the interatrial septum and close to the posterior wall (Fig. 3). Cardiac catheterization showed no pulmonary hypertension and a pulmonary artery wedge pressure of 12 mm Hg, which was the upper limit of normal.

We had previously experienced another teenager who was completely asymptomatic but became severely ill from acute pulmonary congestion immediately after a

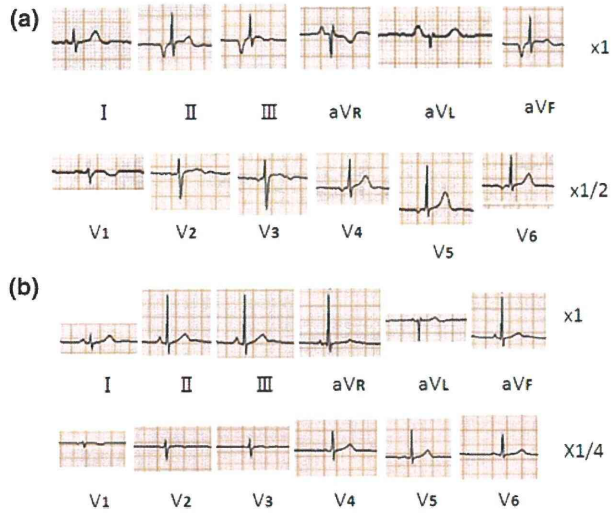

Fig. 1 **a** Before surgery. Negative P waves in *II*, *III*, *aVf*, *V5* and *V6*. **b** 6 months after surgery. Normal P waves with regular rhythm

competitive sport activity [12]. This patient had morphologic characteristics of the anomalous membrane almost identical to those of the reported patient.

In this experience, we performed surgical removal of the anomalous membrane after obtaining an informed consent. Intraoperative direct observation confirmed that the opening was slit-like in shape and located in close proximity to the interatrial septum, with a long axis of 7 mm, which was the same as that measured preoperatively by echocardiography. The operation and the postoperative course were uneventful, and the ECG after the operation showed normal P waves (Fig. 1b).

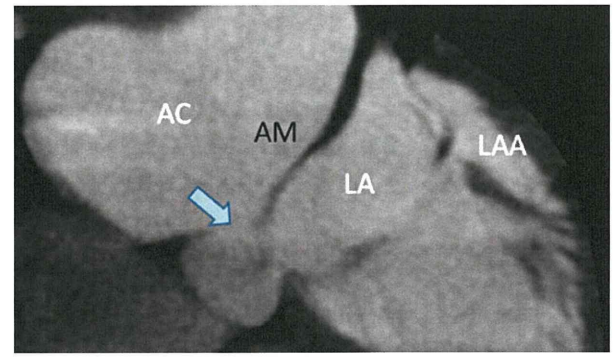

Fig. 3 The anomalous membrane (*AM*) separated the accessory chamber (*AC*) from the left atrium (*LA*). The opening (*arrow*) in the membrane is located along the interatrial septum. *LAA* left atrial appendage

The removed membrane was examined histologically. Hematoxylin-eosin (H&E) staining (Fig. 4a) showed a group of myocardial cells (shown by a star) and two bunches of node-like tissue (shown by yellow arrows). These node-like tissues and the cells around them consisted of cells larger than the working myocardial cells, and their cytoplasm was clear and bright, indicating that these cells were the specialized myocardial cells.

Next, we stained the tissue using Victoria blue-van Gieson (VBG), which indentifies elastic fibers, collagen fibers, and the working myocardial cells. We found that a bunch of clear cells (yellow arrow) was surrounded by fiber tissue and that there were many cells with clear and bright cytoplasm (blue arrows). These portions and cells (indicated by arrows) were negative for the VBG staining,

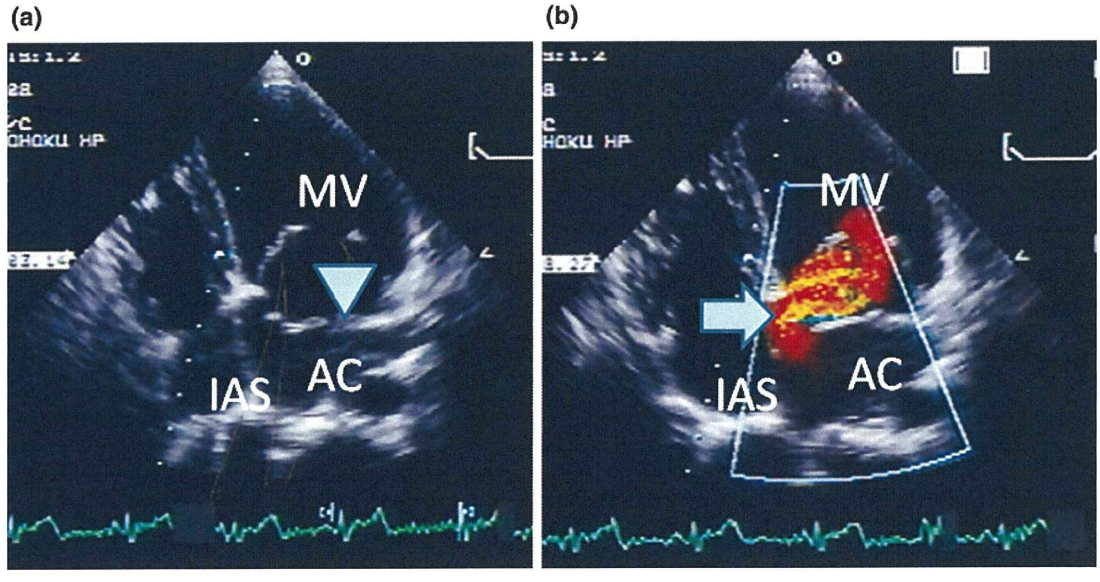

Fig. 2 **a** The anomalous membrane (*inverted triangle*) is visible in 4 chamber view. **b** Color Doppler echocardiogram. Blood stream (*arrow*) from the accessory chamber (*AC*) into the left atrium toward the mitral valve (*MV*) along the interatrial septum (*IAS*)

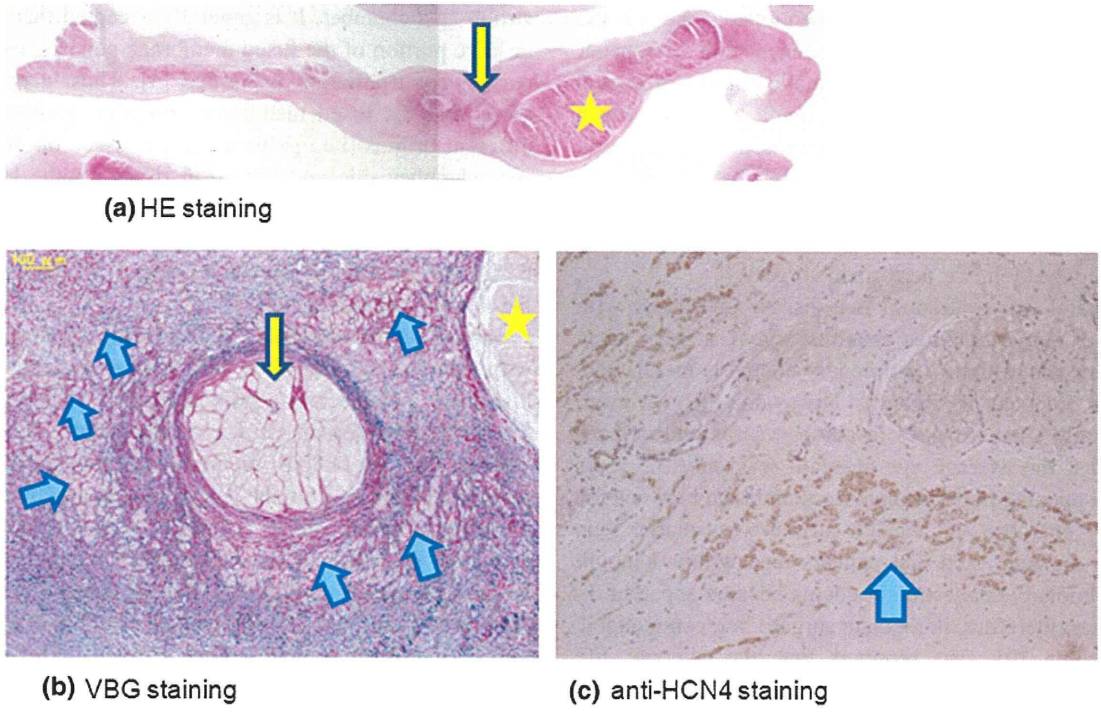

Fig. 4 **a** Hematoxylin-Eosin staining: In the areas (indicated by an *arrow*), there are a bunch of cells, which are larger than the normal myocardial cells and their cytoplasm is bright and clear. The finding indicates that these cells are specialized myocardial cells. The large mass seen at the right part in this section (indicated by a *star*) is a characteristic feature of the working myocardium. **b** Victoria blue-van Gieson (VBG) staining This is magnified figure of the area which is indicated by the *yellow* arrow in **a**. The cells, which were suspected to be specialized myocardial cells by HE staining (*blue arrows*), were not stained by VBG, excluding a possibility that these cells were working myocardial muscle cells, elastic fibers, and/or collagen fibers. And, cells, surrounded by fibers (*yellow arrow*), were also not stained by VBG. **c** Anti-HCN4 antibody staining. This section was almost same as **b**. The HCN-positive cells are those which are presumed by H-E staining to be specialized myocardial cells or cells of the conduction system. This indicates that these cells very likely pose the pacemaker action. *HCN4* hyperpolarization-activated cyclic nucleotide-gated potassium channel 4

indicating that they likely were the specialized myocardial cells.

We then performed immunohistologic staining using antihyperpolarization-activated cyclic nucleotide-gated potassium channel 4 (HCN4) antibody, known to be a marker for the sinoatrial node [1, 8, 10, 11]. The HCN4-positive cells coincided with the cells that seemed to be the specialized myocardial cells by H&E and VBG staining. Thus, we considered that these HCN4 positive cells were the cells of sino-atrial node (SAN) or SAN-like cells, or at least cells with electrical automaticity.

Discussion

Cor triatriatum is relatively rare, occurring at the rate of 0.1–0.4% of all congenital heart disease [3]. This anomaly often presents during infancy, with symptoms and signs caused by pulmonary congestion such as feeding difficulty, poor weight gain, dyspnea, and/or repeated respiratory infections. After infancy, however, cor triatriatum becomes clinically apparent as exertional dyspnea, exercise intolerance or easy fatigability, or even cyanosis with strenuous exercise. However, it may be totally asymptomatic as in our patient, and the diagnosis of asymptomatic patients usually occurs incidentally during an ECG or medical checkup for other reasons.

The diseases presenting with abnormal P wave include heterotaxia syndrome such as polysplenia or left isomerism syndrome [7] and others. Momma et al. [7] investigated the P wave in 50 patients with polysplenia and found a normal P wave in only one patient. Even if the case is not complicated with a hemodynamically significant intracardiac anomaly, polysplenia or left isomerism is known to be associated with sick sinus syndrome or advanced atrioventricular block as patients become older [5]. Thus, to exclude abnormalities associated with the abnormal P waves, we performed echocardiography and as a result found cor triatriatum.

The observed marginal dilation of the pulmonary veins together with the pulmonary wedge pressure at the upper limit of normal range indicated that there was subtle

pulmonary congestion. As we mentioned, one of the authors (M.N.) had previous experience with a teenager who had been completely asymptomatic until he presented suddenly with severe pulmonary edema while playing a badminton game at a tournament representing his school. He underwent emergency surgery, and the morphologic finding was identical to that of the reported case. With this experience and the findings suggestive of the subtle pulmonary congestion, we performed surgery.

In general, cor triatriatum is a disease presenting with pulmonary congestion that requires urgent surgery when pulmonary congestion or pulmonary edema is manifested, which is frequent in infancy. Niwayama [9] reviewed morphologic characteristics in autopsy cases and demonstrated that the average age at death was only 3.3 years when the opening in the anomalous membrane between the accessory chamber and the left atrium was smaller than 3 mm in diameter, and that patients died within 1 month when pulmonary congestion or edema became apparent. In these cases, therefore, immediate surgery is recommended.

Niwayama [9] also reported that the average life expectancy was 16 years if the opening was larger than 3 mm in diameter. The 7-mm opening and the asymptomatic status of our patient seemed to be in accordance with the literature.

The most important and specific point is the presence of electrically active cells in the excised abnormal membrane. We suspected this possibility because the preoperative abnormal P waves were normalized after excision of the membrane. As expected, immunohistologic examination by staining with anti-HCN4 antibody showed a bunch of the staining positive cells in the excised membrane. Reports describe HCN4 staining as a marker of the sinoatrial node in the rat and the rabbit [1, 10, 11]. However, there has been no report on the human, so our result did not definitely confirm that these cells are truly the sinoatrial node cells. However, our finding suggests that the anti-HCN4 antibody positive cells are cells with ability to generate pacemaker action potential in the human even if it is not the sinoatrial node. Moreover, these cells were not stained by VBG, which eliminated the conclusion that they were not elastic fibers, collagen fibers, or working myocardial cells. The results of these two methods suggest that the cell group stained by anti-HCN4 antibody and not by VBG is very likely the sinoatrial node tissue or at least cells with electrical automaticity.

During the early stages of cardiovascular morphogenesis, the common pulmonary vein primordium fuses with the posterior wall of the left atrium. At the beginning, the common pulmonary vein chamber is separated from the left atrium by the fused membrane. Then in the normal process, the fused membrane disappears, causing the common pulmonary vein to be incorporated into the left atrium as a chamber. It is generally accepted that if a part or large portion of the fused membrane persists from some reason, cor triatriatum is formed [4]. Thus, a possibility exists that the fused membrane comprises tissues of two different origins (i.e., pulmonary vein tissue on the accessory chamber side and left atrial tissue on the left atrial side). It is possible that both tissues have cells with pacemaker action. Left atrial rhythm is seen in patients who have congenital heart disease with situs solitus or even in the normal population.

Regarding the pulmonary vein side, the presence of cells with electrical automaticity has been confirmed by both histologic and electrophysiologic studies in recent years [2, 6]. In our patient, it was not possible to ascertain whether the anomalous membrane originated from the pulmonary vein or from the left atrium because the excised tissue appeared as a mass. Therefore, we were not able to ascertain the origin of the cells with pacemaker activity. Regardless of their origin, we showed that the anomalous membrane consisted of cells with pacemaker activity and that the presence of these cells coincided with the anomalous P wave suggestive of left atrial origin, which disappeared after removal of the membrane, resulting in the normal P wave. The reported case showed that the left atrial rhythm or junctional rhythm shown on ECG could be a sign of cor triatriatum.

Acknowledgment The authors acknowledge Drs. Shigehiro Morishima, M.D. and Takashi Ono, M.D. for the operation and Dr Hideo Sakuma, M.D. for the pathologic analysis. This work was supported by an intra-institutional fund.

References

1. Biel M, Schneider A, Wahl C (2002) Cardiac HCN channels: structure, function, and modulation. Trends Cardiovasc Med 12:206–212
2. Chen SA, Hsieh MH, Tai CT et al (1999) Initiation of atrial fibrillation by ectopic beats originating from the pulmonary veins: electrophysiological characteristics, pharmacological responses, and effects of radiofrequency ablation. Circulation 18:1879–1886
3. Geva T, Van Praagh S (2008) Anomalies of the pulmonary veins. In: Allen HD, Driscoll DJ, Shaddy RE, Feltes TF (eds) Moss and Adams' heart disease in infants Children and adolescents. Wolters Kluwer/Lippincott Williams & Wilkins, Philadelphia, pp 761–792
4. Gharagozloo F, Bulkley BH, Hutchins GM (1977) A proposed pathogenesis of cor triatriatum. Am Heart J 94:618–626
5. Gilljam T, Freedom RM, Yoo SJ (2004) The syndrome of isomeric left atrial appendages, often associated with polysplenia. In: Freedom RM, Yoo SJ, Mikailian HJ, Williams WG (eds) The natural and modified history of congenital heart disease. Blackwell, Oxford, pp 430–434
6. Haissaguerre M, Jais P, Shah DC et al (1998) Spontaneous initiation of atrial fibrillation by ectopic beats originating in the pulmonary veins. N Engl J Med 10:659–666

7. Momma K, Takao A, Shibata T (1990) Characteristics and natural history of abnormal atrial rhythms in left isomerism. Am J Cardiol 65:231–236
8. Moosmang S, Stieber J, Zong X et al (2001) Cellular expression and functional characterization of four hyperpolarization-activated channels in cardiac and neuronal tissues. Eur J Biochem 268:1646–1652
9. Niwayama G (1960) Cor triatriatum. Am Heart J 59:291–317
10. Shi W, Wymore R, Yu H et al (2002) Distribution and prevalence of hyperpolarization-activated cation channels (HCN) mRNA expression in cardiac tissues. Circ Res 85:e1–e6
11. Stieber J, Herrmann S, Feil S et al (2003) The hyperpolarization-activated channel HCN4 is required for the generation of pacemaker action potentials in the embryonic heart. Proc Natl Acad Sci USA 215:15235–15240
12. Uemura M, Nishibatake N, Nakazawa M et al (1988) Clinical aspect of cor triatriatum. Acta Paediatr Japonica 92:1294–1300

Arteriosclerosis, Thrombosis, and Vascular Biology

JOURNAL OF THE AMERICAN HEART ASSOCIATION

Xanthine Oxidoreductase Is Involved in Macrophage Foam Cell Formation and Atherosclerosis Development

Akifumi Kushiyama, Hirofumi Okubo, Hideyuki Sakoda, Takako Kikuchi, Midori Fujishiro, Hirokazu Sato, Sakura Kushiyama, Misaki Iwashita, Fusanori Nishimura, Toshiaki Fukushima, Yusuke Nakatsu, Hideaki Kamata, Shoji Kawazu, Yukihito Higashi, Hiroki Kurihara and Tomoichiro Asano

Arterioscler Thromb Vasc Biol. 2012;32:291-298; originally published online November 17, 2011;
doi: 10.1161/ATVBAHA.111.234559
Arteriosclerosis, Thrombosis, and Vascular Biology is published by the American Heart Association, 7272 Greenville Avenue, Dallas, TX 75231

Print ISSN: 1079-5642. Online ISSN: 1524-4636

Xanthine Oxidoreductase Is Involved in Macrophage Foam Cell Formation and Atherosclerosis Development

Akifumi Kushiyama, Hirofumi Okubo, Hideyuki Sakoda, Takako Kikuchi, Midori Fujishiro, Hirokazu Sato, Sakura Kushiyama, Misaki Iwashita, Fusanori Nishimura, Toshiaki Fukushima, Yusuke Nakatsu, Hideaki Kamata, Shoji Kawazu, Yukihito Higashi, Hiroki Kurihara, Tomoichiro Asano

Objective—Hyperuricemia is common in patients with metabolic syndrome. We investigated the role of xanthine oxidoreductase (XOR) in atherosclerosis development, and the effects of the XOR inhibitor allopurinol on this process.

Methods and Results—Oral administration of allopurinol to ApoE knockout mice markedly ameliorated lipid accumulation and calcification in the aorta and aortic root. In addition, allopurinol treatment or siRNA-mediated gene knockdown of XOR suppressed transformation of J774.1 murine macrophage cells, treated with acetylated LDL or very low density lipoprotein (VLDL) into foam cells. This inhibitory effect of allopurinol was also observed in primary cultured human macrophages. In contrast, overexpression of XOR promoted transformation of J774.1 cells into foam cells. Interestingly, SR-A1, SR-B1, SR-B II, and VLDL receptors in J774.1 cells were reduced by XOR knockdown, and increased by XOR overexpression. Conversely, expressions of ABCA1 and ABCG1 were increased by XOR knockdown and suppressed by XOR overexpression. Finally, productions of inflammatory cytokines accompanied by foam cell formation were also reduced by allopurinol administration.

Conclusion—These results strongly suggest XOR activity and/or its expression level to contribute to macrophage foam cell formation. Thus, XOR inhibitors may be useful for preventing atherosclerosis. (***Arterioscler Thromb Vasc Biol.* 2012; 32:291-298.**)

Key Words: atherosclerosis ■ cell physiology ■ cytokines ■ macrophages ■ xanthine oxidoreductase

A relationship between serum uric acid levels and atherosclerotic disease development has been suggested.[1–3] In addition, there is epidemiological evidence of an association between hyperuricemia and metabolic syndrome,[1] type 2 diabetes,[4] chronic kidney diseases,[5,6] heart failure incidence in older adults,[7] and with mortality in patients undergoing percutaneous coronary intervention or with acute myocardial infarction.[8–10] Uric acid itself reportedly functions as an antioxidant,[11] though the process of uric acid synthesis is accompanied by the generation of reactive oxygen species.

Xanthine oxidoreductase (XOR) is a key enzyme in the uric acid production pathway; XOR oxidizes hypoxanthine from nucleic acid metabolites into xanthine, and xanthine into uric acid. XOR basically oxidizes a variety of purines and pterins, classified as molybdenum iron-sulfur flavin hydroxylases. XOR tissue and cellular distributions are high in the mammalian liver and intestine due to XOR-rich parenchymal cells.[12] XOR activity is low in human serum, brain, heart, and skeletal muscle, though a recent study revealed microvascular endothelial cells to be rich in XOR activity.[13] It seems that XOR does not induce harmful reactive oxygen species production under normal conditions but in pathological states such as ischemic congestive heart failure, XOR activity increases drastically and XOR localizes within CD68 positive macrophages.[14] Allopurinol, a xanthine oxidase (XO) inhibitor, has been widely used for hyperuricemia treatment. Oxypurinol, a hydroxide and the main metabolite of allopurinol generated by XOR, covalently binds to XOR and thereby inhibits its activity.[15] Allopurinol reportedly ameliorates chronic stable angina[16] and protects the heart during ischemic reperfusion,[17] and oxypurinol improves the left ventricular ejection fraction in congestive heart failure patients with low left ventricular ejection fraction.[18] It was also suggested that XO inhibitors improve endothelium-dependent vascular relaxation in blood vessels of hyperlipidemic rabbits.[19]

Macrophages play key roles in atherosclerosis development. Macrophages migrate into pathological lesions such as dysfunctional endothelium and then develop into foam cells,

Received on: July 12, 2011; final version accepted on: November 7, 2011.

From the Department of Metabolic Diseases (A.K., T.K., H.S., S.K.), The Institute for Adult Diseases, Asahi Life Foundation, Tokyo, Japan; Department of Medical Chemistry (H.O., M.I., F.N., T.F., Y.N., H.K., Y.H., T.A.), Division of Molecular Medical Science, Graduate School of Biomedical Sciences, Hiroshima University, Hiroshima, Japan; Department of Internal Medicine (H.S., M.F.), Graduate School of Medicine, University of Tokyo, Tokyo, Japan; Department of Physiological Chemistry and Metabolism (S.K., H.K.), Graduate School of Medicine, The University of Tokyo, Tokyo, Japan.

Akifumi Kushiyama and Hirofumi Okubo contributed equally to this study.

Correspondence to Tomoichiro Asano, 1-2-3 Kasumi, Minami-ku, Hiroshima, 734-8553, Japan. E-mail asano-tky@umin.ac.jp

Arterioscler Thromb Vasc Biol **is available at http://atvb.ahajournals.org** **DOI: 10.1161/ATVBAHA.111.234559**

which contribute to vascular stenosis and plaque instability. Foam cell formation by macrophages is accelerated by several extracellular factors, ie, LDL, especially modified LDL,[20] such as oxidized LDL or acetyl LDL (AcLDL), very low density lipoprotein (VLDL),[21] and saturated free fatty acids, as well as by cellular mechanisms such as lipid uptake, metabolism, and efflux. The serum of Watanabe heritable hyperlipidemic rabbits (WHHL), characterized by a mutated LDL receptor, also reportedly induces macrophage foam cell formation.[22,23] Moreover, foam cells secrete cytokines such as tumor necrosis factor (TNF)-α, interleukin (IL)-6 and IL-1β,[24] inducing cellular migration and apoptosis, which also contribute to the development of unstable plaques. The relationships between uric acid metabolism and atherosclerosis and their underlying mechanisms have yet to be elucidated. We thus investigated the effects of XOR and an inhibitor, allopurinol, on atherosclerosis development, focusing especially on effects on macrophages.

Materials and Methods

Animals

This study was approved by the Ethics Committee of the Institute for Adult Diseases, Asahi Life Foundation. All animal experiments were conducted in accordance with the Guidelines for the Care and Use of Laboratory Animals of the same institution. ApoE knockout (KO) mice (B6.129P2-Apoe^{tm1Unc}/J) were purchased from Charles River Co. (Wilmington, MA). All mice were maintained under pathogen-free conditions and a 12-hour light/dark cycle with free access to food and water. The 9-month-old ApoE KO mice were given water either with or without 10 μmol/L allopurinol for 4 weeks, as previously described.[25] The water was replaced every 2 days. Food was withdrawn 12 hours before the experiment.

Preparation of Tissue Samples for Histological Analysis

Nine-month-old mice, with and without allopurinol administration, were euthanized. The heart and entire aorta were removed en bloc and then formalin-fixed. Samples were rinsed with phosphate-buffered saline and aortic roots were routinely embedded in OTC compound (Sakura Finetek Japan, Tokyo, Japan). Sequential 5-μm slices of the aortic root were obtained. The aortic tree was incised longitudinally and then rinsed with phosphate-buffered saline.

Histological Analysis

The aortic root slices and opened aortic trees were stained with oil red O, as previously described.[26] Aortic root slides were counterstained with hematoxylin. In addition, these samples were processed for immunofluorescent staining with antimacrophage antibody (Ab) (1:200, Abcam #56297, Cambridge, UK), and Alexa-fluor488-labeled anti-rat IgG (1:250, Invitrogen, CA). DAPI staining was used to detect the nuclei. Digital images of lesions were obtained with a Nikon Eclipse 50 microscope.

Areas of calcification and lipid accumulation as well as those of macrophage accumulation were histomorphometrically analyzed using MultiGauge ver. 3.1 (FujiFilm, Tokyo, Japan), according to the manufacturer's instructions. The ratios of the lesion area stained by oil red O and that of macrophage accumulation, to the whole aortic wall area and the arterial wall area, respectively, were calculated. In addition, the ratios of calcified or lipid accumulation areas to the whole aortic wall surface were similarly calculated.

Serum Investigation

Serum triglyceride (TG), cholesterol, free fatty acids, and uric acid were assayed with the Triglyceride E test, Cholesterol E test, HDL Cholesterol E test, NEFA C test, and UA C test (all from Wako Chemicals, Osaka, Japan), respectively, according to the manufacturer's instructions. LDL cholesterol (cLDL) was calculated by the Friedewald formula as previously described.[27]

Reagents and Cell Culture

The murine macrophage J774.1 cell line was purchased from Riken (Tsukuba, Japan), cultured in RPMI 1640 (Sigma-Aldrich, St. Louis, MO) medium supplemented with 10% fetal calf serum (Invitrogen), penicillin 100 U/mL, and streptomycin 100 μg/mL (Invitrogen) at 37°C in 5% CO_2. Allopurinol and all reagents were of analytic grade. Lipopolysaccharide (LPS) from Escherichia coli 0111: B4 was purchased from Sigma-Aldrich Japan. Serum of 3-month-old WHHL rabbits was purchased from Oriental Yeast (Tokyo, Japan). Primary Ab for western blotting and immuno-fluorescent staining were purchased, as follows: anti-XOR (Santa Cruz Biotechnology, CA, #sc-20991), LDLR (Cayman Chemical, MI, #1007665), VLDL receptors, SR-A1 (R&D Systems, MN, #AF2258, 1797), CD36 (Lifespan Bioscience, WA, #LS-B662/10019), SR-B1, -B2, ABCG1 (Novus Biologicals, CO, #NB400–101, 102, 132) and ABCA1 (Thermo Scientific, MA, #PA1-16789).

Isolation and Purification of Primary Human Macrophages

To obtain monocytes/macrophages, we isolated peripheral blood mononuclear cells were isolated from 20 mL of blood by centrifugation over a density gradient using Ficoll-Paque PREMIUM (GE Healthcare Japan, Tokyo, Japan). Peripheral blood mononuclear cells were resuspended in 10 mL of RPMI 1640 medium containing 10% fetal bovine serum and purified using MSP-P (JIMRO, Gunma, Japan) according to the manufacturer's instructions. The primary human macrophages obtained were spread onto 24-well culture plates. The indicated concentration of allopurinol was added to the medium 2 hours prior to additional incubation with 50 μg/mL AcLDL (COSMO-Bio, Tokyo, Japan) for 24 hours. After incubation with or without allopurinol or AcLDL, the cells were stained with AdipoRed according to the manufacturer's instructions. Lipid accumulation in macrophages was visualized with a Leica DMIRB microscope.

Quantification of Lipid Accumulation in Macrophages

J774.1 cells were cultured at 90% confluence on 96-well or 12-well plates for lipid accumulation assays as previously described.[28] The indicated concentration of allopurinol was added to the medium 2 hours prior to additional incubation with 10 ng/mL LPS, 1% WHHL rabbit serum, 50 μg/mL AcLDL or 50 μg/mL VLDL, for 24 hours. The cells were then stained with AdipoRed and visualized with a Leica DMIRB microscope, or subjected to lipid accumulation quantification using an ARVO MX fluorimeter (PerkinElmer, MA), according to the manufacturer's instructions.

DiI AcLDL Uptake Assay

For the DiI (3,3′-dioctadecylindocarbocyanine)-AcLDL uptake assay, 50 μg/dL DiI AcLDL were added to RPMI 1640 medium containing the indicated concentrations of WHHL rabbit serum and allopurinol. Then the cells were incubated for another 4 hours, and finally rinsed twice with phosphate-buffered saline. Cellular DiI-AcLDL uptake was then measured using the ARVO MX fluorimeter.

Overexpression of XOR and Knockdown of XOR

The cDNA encoding mouse XOR was obtained from Kazusa DNA Research Institute (Chiba, Japan). XOR cDNA and control LacZ cDNA were each inserted into pcDNA3.1(+) plasmids. The siRNAs of XOR and the control were purchased from Invitrogen (XOR siRNA #1320003 MSS238717, control siRNA HiGC 12935-400). Lipofection of cDNA plasmids or siRNA was performed using FuGene HD (Roche, Basel, Switzerland) or lipofectamine RNAiMAX (Invitrogen), respectively, according to the manufacturer's instructions.

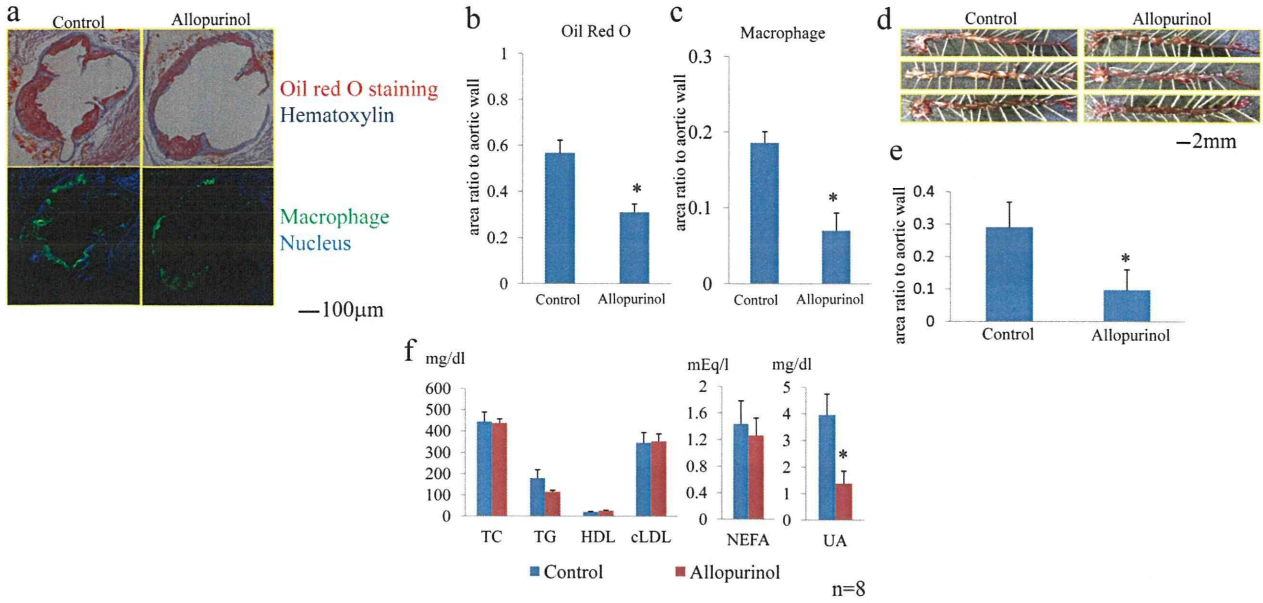

Figure 1. The in vivo effect of allopurinol against atherosclerotic lesion development. **a**, Oil red O staining and macrophage immunostaining of the aortic roots of 9-month-old ApoE knockout (KO) mice with and without allopurinol administration. Upper panels show Oil Red O staining and counterstaining with hematoxylin. Lower panels show macrophage immunostaining (**Green**) and counterstaining with DAPI (**Blue**). **b**, Quantification of lesion area, stained with Oil Red O. Mean±SE. The ratio of the stained lipid area to the arterial wall area is presented. **c**, Quantification of immunostained macrophage area. Mean±SE. The ratio of the stained macrophage area to the arterial wall area is presented. **d**, Oil red staining of incised aortic wall throughout the aortic tree. Lipid accumulation including the area of calcification is stained orange. **e**, Quantification of lesion area, stained with Oil Red O. Mean±SE. The ratio of the stained lipid and calcified area to the arterial wall inner surface is presented. **f**, Serum examinations of ApoEKO mice with and without allopurinol administration. cLDL indicates calculated LDL; TC, total cholesterol; TG, triglyceride; NEFA, non-esterified fatty acid; UA, uric acid. The asterisk (*) indicates statistical significance at $P<0.05$.

Western Blotting

Western blot analysis was carried out as described previously.[29] In brief, 10 μg of protein were separated by SDS-PAGE and electrophoretically transferred to membranes, which were then incubated with specific Ab. The antigen-Ab interactions were visualized using HRP-conjugated secondary Ab and SuperSignal West Pico Chemiluminescent Substrate (Thermo Scientific). Band images were obtained with LAS-4000 (FujiFilm) and quantified using MultiGauge ver. 3.1. Fold changes in protein expressions, as compared to β-actin, were determined in triplicate.

Quantification of Cytokine Expressions

J774.1 cells were cultured in RPMI 1640 with 10% FCS. The indicated concentration of allopurinol was added to the medium 2 hours prior to additional incubation with 10 ng/mL LPS or 1% WHHL rabbit serum for 24 hours. Then, mRNA was prepared from the cells using an RNeasy-mini kit (QIAGEN, Hilden, Germany) according to the manufacturer's instructions and 1 μg of this mRNA was reverse transcribed with Transcriptor Reverse Transcriptase (Roche). Quantitative real-time PCR was run with a LightCycler480 (Roche Diagnosis Japan) using FastStart SYBR Green Master (Roche). The primers were designed as follows: mouse IL-1β forward, 5′-TCGCTCAGGGTCACAAGAAA-3′, mouse IL-1β reverse, 5′-CATCAGAGGCAAGGAGGAAAAC-3′, mouse IL-6 forward, 5′-GATGCTACCAAACTGGATATAATC-3′, mouse IL-6 reverse, 5′-CTGGCACCACTAGTTGGTTGTC-3′, mouse TNF-α forward, 5′-GCCACCACGCTCTTCTGTCT-3′, mouse TNF-α reverse, 5′-GTCTGGGCCATAGAACTGAT-3′, mouse actin forward, 5′-ATCATTGCTCTCCTGAGCG-3′, mouse actin reverse, 5′-GCTGATCCACATCTGGAA-3′. Post-PCR melting curves confirmed the specificity of single-target amplification. Relative gene expressions were calculated by the efficiency correction method.[30] Fold changes in the expressions of IL-1β, IL-6, IL-12, and TNF-α normalized by the actin level were determined in triplicate.

Statistical Analysis

Results are presented as means±SE. ANOVA and Student t test were used for parametric data, the Mann-Whitney U test for nonparametric data. Statistical significance was $P<0.05$.

Results

In Vivo Quantification of Atherosclerotic Plaque in ApoE KO Mice

A 10 μmol/L dose of allopurinol was administered daily for 4 weeks to 9-month-old ApoE KO mice (n=8). Oil red O staining revealed markedly reduced lipid accumulation in the aortic roots of allopurinol-treated ApoE KO mice (upper panels of Figure 1a), quantified as a 45.5% reduction in lipid droplets as compared with control ApoE KO mice (Figure 1b). Numbers of macrophages in aortic sections were also significantly lower, as shown by immunostaining (lower panels of Figure 1a), and quantification revealed a 72.2% reduction in the macrophage accumulation area (Figure 1c). The area of calcification in the aorta (Figure 1d) was also estimated and revealed a 67.0% reduction in the allopurinol-treated group, as compared with the control (Figure 1e). In allopurinol-treated mice, serum TG levels were slightly lower than in control mice, but this difference was not statistically significant (Figure 1f). Serum uric acid was reduced by 65.1%, whereas serum concentrations of total cholesterol, HDL, cLDL, and free fatty acids did not differ between the allopurinol-treated and control groups (1f). There were no differences in body weight between the 2 groups throughout the study period

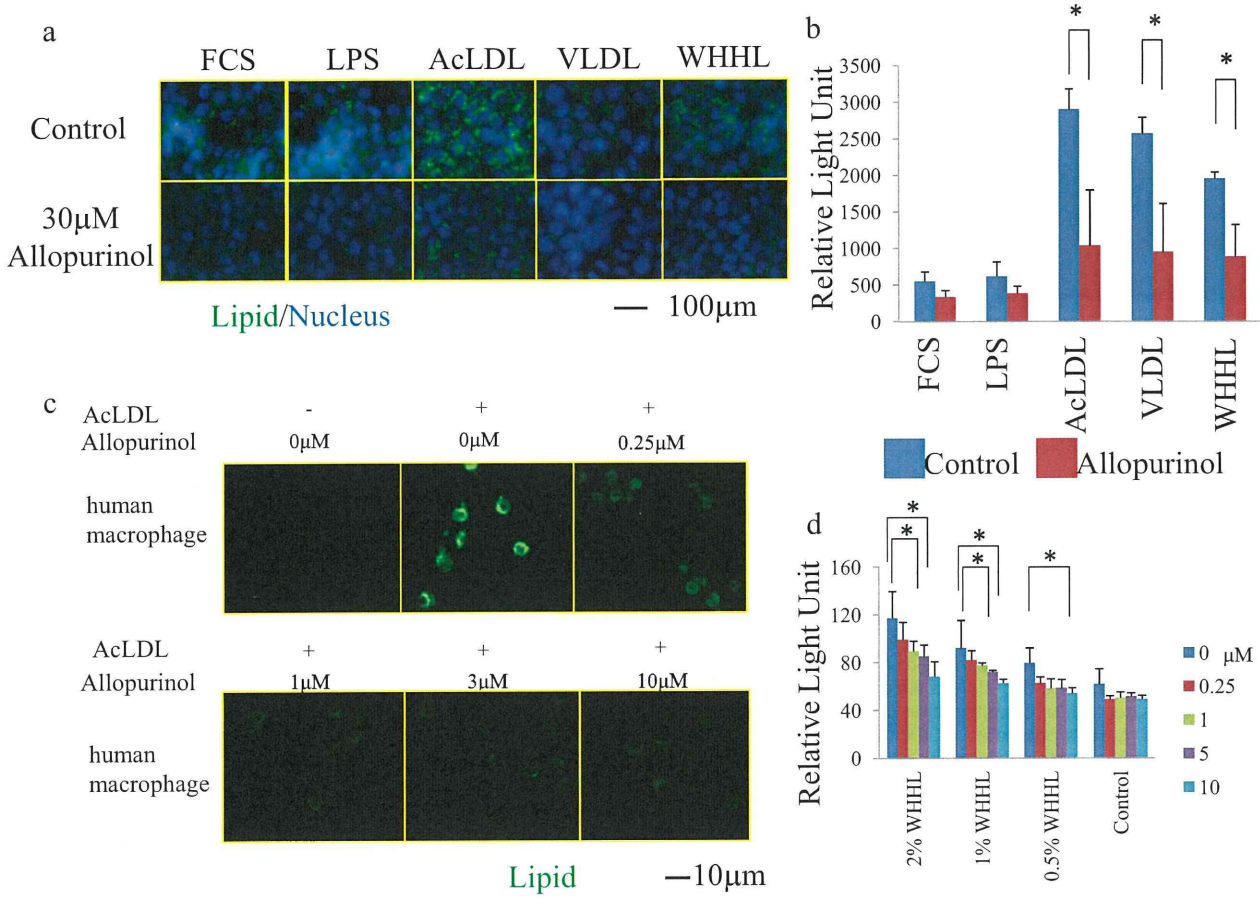

Figure 2. Lipid accumulation within J774.1 cells and human isolated macrophages. **a**, AdipoRed staining was performed and lipid accumulation was quantified. The effects of 30 μmol/L allopurinol on lipid accumulation in J774.1 cells induced by 10 ng/mL LPS, 50 μg/mL acetyl LDL (AcLDL), 50 μg/dL VLDL, and 1% WHHL rabbit serum are shown. Cellular lipid is stained green by AdipoRed, the nucleus is stained blue by DAPI. **b**, Quantification of cellular lipids stained by AdipoRed, induced as in 2a. The asterisk (*) indicates statistical significance at $P<0.05$. **c**, AdipoRed staining was performed on human isolated macrophages treated with 50 μg/mL AcLDL for 24 hours. The indicated concentration of allopurinol was added 2 hours prior to AcLDL incubation. Cellular lipid is stained green by AdipoRed. **d**, Assay of DiI AcLDL uptake. The effect of allopurinol administration on AcLDL uptake was quantified. LPS indicates lipopolysaccharide; VLDL, very low density lipoprotein; WHHL, Watanabe heritable hyperlipidemic rabbits.

(data not shown). Thus, allopurinol markedly suppressed atherosclerosis in vivo without significantly altering cholesterol levels.

In Vitro Quantification of Macrophage Foam Cell Formation

J774.1 cells were incubated with 10 ng/mL LPS, 50 μg/mL AcLDL, 50 μg/mL VLDL, or 1% WHHL rabbit serum in the absence or presence of the indicated allopurinol concentrations (Figure 2a and 2b). Transformation of J774.1 cells into lipid-containing foam cells was examined by Adipored staining, followed by quantification. It was revealed that allopurinol reduced lipid accumulation in J774.1 cells, induced by AcLDL, VLDL, or WHHL rabbit serum. LPS treatment for 24 hours did not affect lipid accumulation in J774.1 cells. Very similarly, allopurinol markedly ameliorated AcLDL-induced lipid accumulation in primary human macrophages (Figure 2c).

Allopurinol Suppresses Uptake of AcLDL Into Macrophages

Because AcLDL-induced transformation of J774.1 cells into foam cells was suppressed, the effect of allopurinol on AcLDL uptake was investigated. The J774.1 cells were incubated with normal or 0.5% to 2% WHHL rabbit serum, in the absence or presence of the indicated allopurinol concentrations. Then, transport of DiI AcLDL into the cells was examined. Allopurinol concentration-dependently inhibited WHHL serum-enhanced DiI AcLDL uptake, but had no effect on that taken up by cells incubated with normal rabbit serum (Figure 2c).

XOR Expression and Lipid Accumulation

Because allopurinol was shown to inhibit lipid accumulation in macrophages, we next examined the effect of XOR overexpression, which resulted in an approximately 1.8-fold increase in total expression of XOR protein, whereas siRNA-mediated gene-knockdown of XOR resulted in a 50% expression reduction (Figure 3a). XOR overexpression exacerbated foam cell formation (Figure 3b and 3c) and increased DiI-AcLDL uptake (Figure 3d) into J774.1 cells, although these reactions were inhibited by XOR knockdown (Figure 3b, 3e, and 3f). XOR overexpression also induced lipid accumulation even in the absence of additional lipids in the medium.

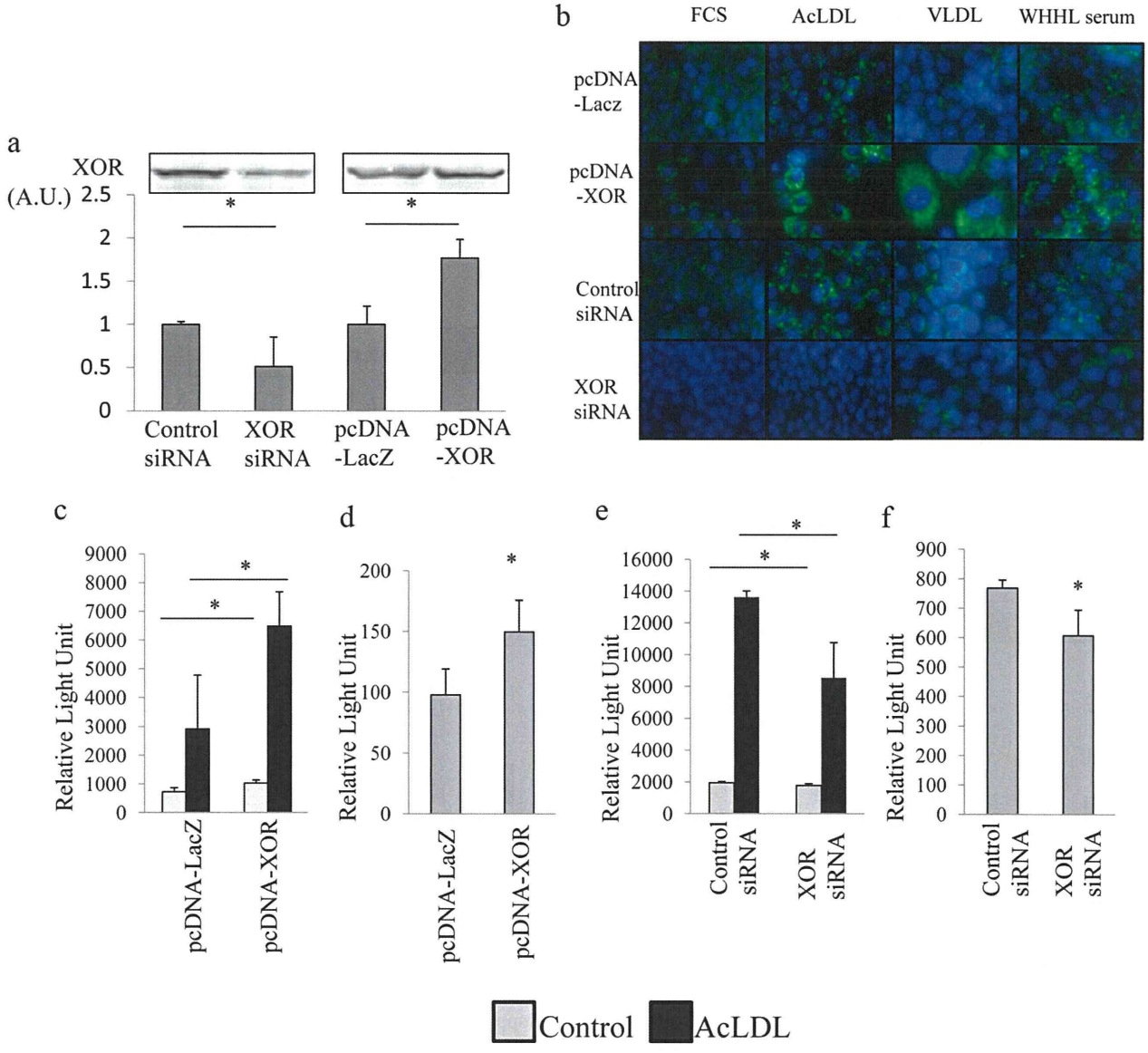

Figure 3. Effects of oxidoreductase (XOR) overexpression and knockdown on foam cell formation. **a**, Western blotting of XOR protein, representative bands and quantified band intensities, presented as means±SE, are shown for samples from J774.1 cell extracts. XOR knockdown mediated by siRNA and overexpression of XOR. Mean±SE of XOR band intensity is shown. **b**, The effects of XOR overexpression or siRNA mediated XOR gene knockdown on lipid accumulation induced by 10 ng/mL LPS, 50 μg/mL acetyl LDL (AcLDL), 50 μg/dL very low density lipoprotein (VLDL), and 1% Watanabe heritable hyperlipidemic rabbits (WHHL) rabbit serum. Cellular lipid is stained green by AdipoRed, the nucleus is stained blue by DAPI. **c** and **e**, Lipid accumulation in J774.1 cells incubated with 1% control rabbit serum or 1% WHHL rabbit serum. The effect of XOR overexpression (**c**) and siRNA-mediated XOR knockdown (**e**) are shown. **d** and **f**, Assays of DiI-AcLDL uptake. The effect of XOR overexpression (**d**) and siRNA-mediated XOR knockdown (**f**) are shown. The asterisk (*) indicates statistical significance at $P<0.05$.

Moreover, XOR overexpression with VLDL incubation induced cellular enlargement and multinucleation (Figure 3b).

Expressions of Lipoprotein Receptors and ABC Transporters Involved in Lipid Transport

XOR overexpression induced expressions of lipoprotein receptors, such as SR-B1, SR-B2, and VLDL. XOR siRNA knockdown diminished CD36, SR-A1, and LDL receptors. With XOR overexpression, ABCA1 and ABCG1 were diminished, whereas XOR knockdown induced expressions of ABC transporters such as ABCA1 and ABCG1 (Figure 4). In support of these data, allopurinol also suppressed lipoprotein receptors and induced ABCA1 and ABCG1 (Supplemental Figure III, available online at http://atvb.ahajournals.org).

Inflammatory Cytokine Secretions and Key Molecules in Atherosclerosis Development

Inflammatory cytokines such as IL-1β, IL-6, IL-12, and TNFα were dose-dependently inhibited by allopurinol when foam cell formation was triggered by WHHL serum (Supplemental Figure IVa–IVd), whereas secretions of LPS-induced cytokines, other than IL-6 (Supplemental Figure IVg), were unaffected by allopurinol (Supplemental Figure IVe, IVf, and IVh). Incubation with WHHL serum induced VCAM1,

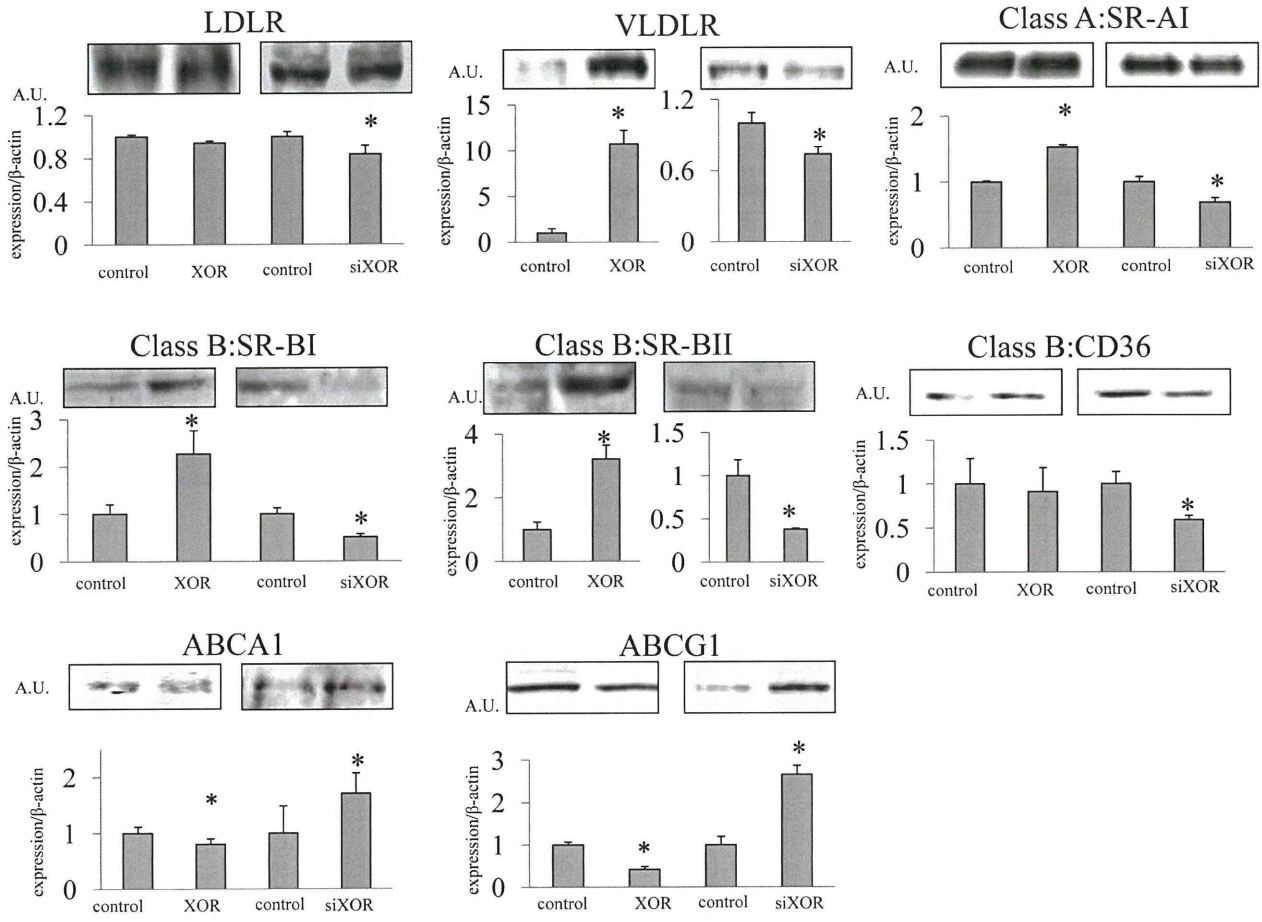

Figure 4. Quantification of lipoprotein receptors and ABC transporters involved in lipid transport with overexpression or suppression of oxidoreductase (XOR) in J774.1 cells. Western blotting was performed using specific antibodies for lipoprotein receptors and ABC transporters involved in lipid transporters. Representative bands and quantified band intensity are presented as means±SE. The asterisk (*) indicates statistical significance at $P<0.05$. LDLR indicates LDL receptor; VLDLR, very low-density lipoprotein receptor.

MCP-1, and MMP2 but neither ICAM1 nor MMP9 expression. Allopurinol suppressed these inductions and inhibited expression of MMP9. LPS induced MCP-1 and MMP2, and these expressions were slightly blunted by allopurinol administration. VCAM1 and MMP9 were suppressed by 10 ng/mL LPS, and adding allopurinol further suppressed both (Supplemental Figure V).

Discussion

This study is the first to show that XOR plays a key role in the transformation of macrophages into foam cells and the development of atherosclerotic plaque. It was clearly demonstrated that oral administration of allopurinol for 4 weeks significantly inhibited lipid accumulation and calcification in the aortas of ApoE KO mice. Interestingly, serum lipid levels were not significantly altered by allopurinol. TG was slightly, but not significantly, reduced. Rats with fructose-induced hyperuricemia given allopurinol had reduced serum TG levels[25] suggesting a weak TG-lowering effect in rodents. In contrast, allopurinol markedly reduced serum uric acid in ApoE KO mice to approximately one-third of normal.

While XOR activity is highest in the liver and intestines, a previous histological study revealed that XOR is also present in macrophages.[14] In good agreement with that report, we observed XOR to be abundant in macrophages clustered at the aortic root (Supplemental Figure IA and IB). Importantly, using XOR overexpression as well as XOR siRNA or allopurinol treatment, we demonstrated XOR activity to be critical for the transformation of J774.1 cells and human macrophages into foam cells. The allopurinol concentration was essentially within physiological range, ie, the trough serum oxypurinol concentration [>4.6 μg/mL (=30.2 μmol/L)] approximated that achieved by a 100 to 200 mg single allopurinol administration to hyperuricemic patients.[31] Thus, our in vitro results might be applicable to clinical practice. XO activation was induced by hypoxia, LPS, hypoxia-inducible factor 1, and inflammatory cytokines like IL-1β.[32] We also found secretion of inflammatory cytokines to be accompanied by foam cell formation, which was blocked by XOR inhibition.

Inflammatory cytokines were induced via XOR when foam cells formed, although not via, at least not entirely, the XOR pathway when stimulated by LPS. These observations suggest a vicious cycle of lipid accumulation and XOR activation to be involved in foam cell formation, which might contribute to the mechanism of plaque development. Phagocytosis was not affected by XOR inhibition (Supplemental Figure II). Thus, phagocytic activity does not involve XOR.

There are reports describing XOR as an endogenous regulator of cyclooxygenase (Cox)-2[33] in the inflammatory system, and XOR appears to be central to innate immune function.[34] In addition, XOR is critically involved in both differentiation and lipid metabolism of adipose tissue. Because XOR is a regulator of adipogenesis and peroxisome proliferator-activated receptor activity, XOR−/− mice demonstrate a 50% reduction in adipose mass versus their littermates.[35] PPARγ also plays roles in macrophage lipid efflux[36] in a manner opposite that of lipid retention. Cox-2 has central roles in innate immunity and inflammation and is regulated by a negative feedback loop mediated by PPARγ.[37] XOR is thought to be upstream from PPARγ in lipid retention[35] and also to induce Cox-2, which then promotes inflammation, also possibly constituting a feedback loop.

In macrophages, cellular mechanisms of lipid metabolism such as lipid influx and efflux are mediated by lipoprotein receptors such as scavenger receptors and some ABC transporters.[38,39] As to scavenger receptors, both class A, especially SR-A1, and class B, such as SR-B1 and -B2, receptors appear to be involved in this XOR system. Class A receptors include SR-A1, SR-A2, MARCO, and SRCL, receptors for oxidized LDL and AcLDL, whereas class B receptors include CD36, SR-B1, and mediators of MAPK or TLR signaling, leading to expressions of inflammatory cytokines and reactive oxygen species generation. Therefore, the SR-B receptor decrease with XOR inhibition observed herein might suppress cytokine expressions. Among proteins involved in lipid uptake, VLDL receptor was strongly induced by XOR overexpression. Although cholesterol efflux was not examined, according to our data, expressions of ABCA1 and ABCG1 were reduced by XOR overexpression. Inflammation reportedly inhibits expressions of these genes.[40,41]

In ApoE KO mice, atherosclerotic plaque was predominantly derived from ApoE deficiency in HDL leading to impaired efflux of cholesterol.[42] Influx of cholesterol in ApoE KO mice depends on high serum cholesterol levels, produced by serum ApoE deficiency,[43] dysfunction of the normal, rapid catabolism of chylomicron remnants entering the liver via ApoE,[44] and evident accumulation of VLDL containing cholesteryl esters.[45] Allopurinol did not change serum cholesterol levels, although XOR expression changed amounts of lipid transporting proteins in macrophages. Thus, the antiatherosclerotic effect of allopurinol is independent of lipoprotein metabolism in the liver and might be directed to macrophages.

A previous report revealed tungsten to prevent atherosclerosis development[46] but did not focus on lipid accumulation in plaque areas or foam cell formation by macrophages. In addition, tungsten inhibits XDH transcription and also proteolytic processing of XDH protein. Thus, proteolytic involvement of tungsten in more proteins than just XDH cannot be ruled out.

A major limitation in applying our results to clinical practice appears to be the differences in XOR distributions among humans and other species, in both physiological and pathophysiological states.[12] These differences are not yet well understood. However, macrophages express XOR and are known to play roles in such disorders as angina, congestive heart failure, and chronic kidney disease, and our results indicate allopurinol is directly and significantly involved in the transformation of macrophages into foam cells.

Although further investigation is needed, our results clearly suggest the importance of inhibiting XO activity for the prevention and treatment of atherosclerosis and may provide insights allowing the development of novel antiatherosclerotic drugs.

Acknowledgments

Akifumi Kushiyama, Hirofumi Okubo, and Tomoichiro Asano designed research; Akifumi Kushiyama, Hirofumi Okubo, Hideyuki Sakoda, Takako Kikuchi, Midori Fujishiro, Hirokazu Sato, Sakura Kushiyama, Misaki Iwashita Yusuke Nakatsu, Fusanori Nishimura, Toshiaki Fukushima, Yukihito Higashi, and Hiroki Kurihara performed research; S.K., Yukihito Higashi, and Hiroki Kurihara analyzed data; and Akifumi Kushiyama and Tomoichiro Asano wrote the paper.

Disclosures

None.

References

1. Ishizaka N, Ishizaka Y, Toda E, Nagai R, Yamakado M. Association between serum uric acid, metabolic syndrome, and carotid atherosclerosis in Japanese individuals. *Arteriosclerosis, Thrombosis, and Vascular Biology*. 2005;25:1038–1044.
2. Silbernagel G, Hoffmann MM, Grammer TB, Boehm BO, Marz W. Uric acid is predictive of cardiovascular mortality and sudden cardiac death in subjects referred for coronary angiography. *Nutrition, Metabolism, and Cardiovascular Diseases: NMCD*. 2011.
3. Rodrigues TC, Maahs DM, Johnson RJ, Jalal DI, Kinney GL, Rivard C, Rewers M, Snell-Bergeon JK. Serum uric acid predicts progression of subclinical coronary atherosclerosis in individuals without renal disease. *Diabetes Care*. 2010;33:2471–2473.
4. Facchini F, Chen YD, Hollenbeck CB, Reaven GM. Relationship between resistance to insulin-mediated glucose uptake, urinary uric acid clearance, and plasma uric acid concentration. *JAMA*. 1991;266:3008–3011.
5. Tanaka K, Hara S, Kushiyama A, Ubara Y, Yoshida Y, Mizuiri S, Aikawa A, Kawatzu S. Risk of macrovascular disease stratified by stage of chronic kidney disease in type 2 diabetic patients: Critical level of the estimated glomerular filtration rate and the significance of hyperuricemia. *Clinical and Experimental Nephrology*. 2011;15:391–397.
6. Ficociello LH, Rosolowsky ET, Niewczas MA, Maselli NJ, Weinberg JM, Aschengrau A, Eckfeldt JH, Stanton RC, Galecki AT, Doria A, Warram JH, Krolewski AS. High-normal serum uric acid increases risk of early progressive renal function loss in type 1 diabetes: Results of a 6-year follow-up. *Diabetes Care*. 2010;33:1337–1343.
7. Ekundayo OJ, Dell'Italia LJ, Sanders PW, Arnett D, Aban I, Love TE, Filippatos G, Anker SD, Lloyd-Jones DM, Bakris G, Mujib M, Ahmed A. Association between hyperuricemia and incident heart failure among older adults: A propensity-matched study. *Int J Cardiol*. 2010;142:279–287.
8. Spoon DB, Lerman A, Rule AD, Prasad A, Lennon RJ, Holmes DR, Rihal CS. The association of serum uric acid levels with outcomes following percutaneous coronary intervention. *J Interv Cardiol*. 2010;23:277–283.
9. Kowalczyk J, Francuz P, Swoboda R, Lenarczyk R, Sredniawa B, Golda A, Kurek T, Mazurek M, Podolecki T, Polonski L, Kalarus Z. Prognostic significance of hyperuricemia in patients with different types of renal dysfunction and acute myocardial infarction treated with percutaneous coronary intervention. *Nephron Clin Pract*. 2010;116:c114–c122.
10. Lazzeri C, Valente S, Chiostri M, Sori A, Bernardo P, Gensini GF. Uric acid in the acute phase of st elevation myocardial infarction submitted to primary pci: Its prognostic role and relation with inflammatory markers: A single center experience. *Int J Cardiol*. 2010;138:206–209.
11. Alvarez-Lario B, Macarron-Vicente J. Uric acid and evolution. *Rheumatology (Oxford)*. 2010;49:2010–2015.
12. Pritsos CA. Cellular distribution, metabolism and regulation of the xanthine oxidoreductase enzyme system. *Chemico-Biological Interactions*. 2000;129:195–208.

13. Moriwaki Y, Yamamoto T, Suda M, Nasako Y, Takahashi S, Agbedana OE, Hada T, Higashino K. Purification and immunohistochemical tissue localization of human xanthine oxidase. *Biochimica et Biophysica Acta.* 1993;1164:327–330.
14. de Jong JW, Schoemaker RG, de Jonge R, Bernocchi P, Keijzer E, Harrison R, Sharma HS, Ceconi C. Enhanced expression and activity of xanthine oxidoreductase in the failing heart. *J Mol Cell Cardiol.* 2000; 32:2083–2089.
15. Massey V, Komai H, Palmer G, Elion GB. On the mechanism of inactivation of xanthine oxidase by allopurinol and other pyrazolo[3,4-d]pyrimidines. *J Biol Chem.* 1970;245:2837–2844.
16. Noman A, Ang DS, Ogston S, Lang CC, Struthers AD. Effect of high-dose allopurinol on exercise in patients with chronic stable angina: A randomised, placebo controlled crossover trial. *Lancet.* 375:2161–2167.
17. Johnson WD, Kayser KL, Brenowitz JB, Saedi SF. A randomized controlled trial of allopurinol in coronary bypass surgery. *Am Heart J.* 1991;121:20–24.
18. Cingolani HE, Plastino JA, Escudero EM, Mangal B, Brown J, Perez NG. The effect of xanthine oxidase inhibition upon ejection fraction in heart failure patients: La plata study. *J Card Fail.* 2006;12:491–498.
19. Ohara Y, Peterson TE, Harrison DG. Hypercholesterolemia increases endothelial superoxide anion production. *J Clin Invest.* 1993;91: 2546–2551.
20. Ishigaki Y, Katagiri H, Gao J, Yamada T, Imai J, Uno K, Hasegawa Y, Kaneko K, Ogihara T, Ishihara H, Sato Y, Takikawa K, Nishimichi N, Matsuda H, Sawamura T, Oka Y. Impact of plasma oxidized low-density lipoprotein removal on atherosclerosis. *Circulation.* 2008;118:75–83.
21. Ito T, Yamada S, Shiomi M. Progression of coronary atherosclerosis relates to the onset of myocardial infarction in an animal model of spontaneous myocardial infarction (whhlmi rabbits). *Exp Anim.* 2004;53: 339–346.
22. Shiomi M, Ito T, Yamada S, Kawashima S, Fan J. Development of an animal model for spontaneous myocardial infarction (whhlmi rabbit). *Arterioscler Thromb Vasc Biol.* 2003;23:1239–1244.
23. Buja LM, Kita T, Goldstein JL, Watanabe Y, Brown MS. Cellular pathology of progressive atherosclerosis in the whhl rabbit. An animal model of familial hypercholesterolemia. *Arteriosclerosis.* 1983;3:87–101.
24. Seneviratne AN, Sivagurunathan B, Monaco C. Toll-like receptors and macrophage activation in atherosclerosis. *Clinica Chimica Acta; International Journal of Clinical Chemistry.* 2011.
25. Nakagawa T, Hu H, Zharikov S, Tuttle KR, Short RA, Glushakova O, Ouyang X, Feig DI, Block ER, Herrera-Acosta J, Patel JM, Johnson RJ. A causal role for uric acid in fructose-induced metabolic syndrome. *Am J Physiol Renal Physiol.* 2006;290:F625–F631.
26. Catalano RA, Lillie RD. Elimination of precipitates in oil red o fat stain by adding dextrin. *Stain Technol.* 1975;50:297–299.
27. Fraulob JC, Ogg-Diamantino R, Fernandes-Santos C, Aguila MB, Mandarim-de-Lacerda CA. A mouse model of metabolic syndrome: Insulin resistance, fatty liver and non-alcoholic fatty pancreas disease (nafpd) in c57bl/6 mice fed a high fat diet. *Journal of Clinical Biochemistry and Nutrition.* 2010;46:212–223.
28. Cui X, Kushiyama A, Yoneda M, Nakatsu Y, Guo Y, Zhang J, Ono H, Kanna M, Sakoda H, Kikuchi T, Fujishiro M, Shiomi M, Kamata H, Kurihara H, Kikuchi M, Kawazu S, Nishimura F, Asano T. Macrophage foam cell formation is augmented in serum from patients with diabetic angiopathy. *Diabetes Res Clin Pract.* 2010;87:57–63.
29. Kushiyama A, Shojima N, Ogihara T, Inukai K, Sakoda H, Fujishiro M, Fukushima Y, Anai M, Ono H, Horike N, Viana AY, Uchijima Y, Nishiyama K, Shimosawa T, Fujita T, Katagiri H, Oka Y, Kurihara H, Asano T. Resistin-like molecule beta activates mapks, suppresses insulin signaling in hepatocytes, and induces diabetes, hyperlipidemia, and fatty liver in transgenic mice on a high fat diet. *J Biol Chem.* 2005;280: 42016–42025.
30. Pfaffl MW. A new mathematical model for relative quantification in real-time rt-pcr. *Nucleic Acids Research.* 2001;29:e45.
31. Takada M, Okada H, Kotake T, Kawato N, Saito M, Nakai M, Gunji T, Shibakawa M. Appropriate dosing regimen of allopurinol in japanese patients. *J Clin Pharm Ther.* 2005;30:407–412.
32. Nicholas SA, Bubnov VV, Yasinska IM, Sumbayev VV. Involvement of xanthine oxidase and hypoxia-inducible factor 1 in toll-like receptor 7/8-mediated activation of caspase 1 and interleukin-1beta. *Cell Mol Life Sci.*
33. Ohtsubo T, Rovira II, Starost MF, Liu C, Finkel T. Xanthine oxidoreductase is an endogenous regulator of cyclooxygenase-2. *Circ Res.* 2004;95:1118–1124.
34. Vorbach C, Harrison R, Capecchi MR. Xanthine oxidoreductase is central to the evolution and function of the innate immune system. *Trends Immunol.* 2003;24:512–517.
35. Cheung KJ, Tzameli I, Pissios P, Rovira I, Gavrilova O, Ohtsubo T, Chen Z, Finkel T, Flier JS, Friedman JM. Xanthine oxidoreductase is a regulator of adipogenesis and ppargamma activity. *Cell Metab.* 2007;5: 115–128.
36. Liu W, He P, Cheng B, Mei CL, Wang YF, Wan JJ. Chlamydia pneumoniae disturbs cholesterol homeostasis in human thp-1 macrophages via jnk-ppargamma dependent signal transduction pathways. *Microbes and Infection/Institut Pasteur.* 2010;12:1226–1235.
37. Inoue H, Tanabe T, Umesono K. Feedback control of cyclooxygenase-2 expression through ppargamma. *The Journal of Biological Chemistry.* 2000;275:28028–28032.
38. Hansson GK, Robertson AK, Soderberg-Naucler C. Inflammation and atherosclerosis. *Annu Rev Pathol.* 2006;1:297–329.
39. Zhao B, Song J, Chow WN, St Clair RW, Rudel LL, Ghosh S. Macrophage-specific transgenic expression of cholesteryl ester hydrolase significantly reduces atherosclerosis and lesion necrosis in ldlr mice. *J Clin Invest.* 2007;117:2983–2992.
40. Panousis CG, Zuckerman SH. Interferon-gamma induces downregulation of tangier disease gene (atp-binding-cassette transporter 1) in macrophage-derived foam cells. *Arterioscler Thromb Vasc Biol.* 2000;20: 1565–1571.
41. Khovidhunkit W, Moser AH, Shigenaga JK, Grunfeld C, Feingold KR. Endotoxin down-regulates abcg5 and abcg8 in mouse liver and abca1 and abcg1 in j774 murine macrophages: Differential role of lxr. *J Lipid Res.* 2003;44:1728–1736.
42. Hayek T, Oiknine J, Brook JG, Aviram M. Role of hdl apolipoprotein e in cellular cholesterol efflux: Studies in apo E knockout transgenic mice. *Biochem Biophys Res Commun.* 1994;205:1072–1078.
43. Kashyap VS, Santamarina-Fojo S, Brown DR, Parrott CL, Applebaum-Bowden D, Meyn S, Talley G, Paigen B, Maeda N, Brewer HB, Jr. Apolipoprotein E deficiency in mice: Gene replacement and prevention of atherosclerosis using adenovirus vectors. *J Clin Invest.* 1995;96: 1612–1620.
44. Mortimer BC, Martins I, Zeng BJ, Redgrave TG. Use of gene-manipulated models to study the physiology of lipid transport. *Clin Exp Pharmacol Physiol.* 1997;24:281–285.
45. Woollett LA, Osono Y, Herz J, Dietschy JM. Apolipoprotein E competitively inhibits receptor-dependent low density lipoprotein uptake by the liver but has no effect on cholesterol absorption or synthesis in the mouse. *Proc Natl Acad Sci U S A.* 1995;92:12500–12504.
46. Schroder K, Vecchione C, Jung O, Schreiber JG, Shiri-Sverdlov R, van Gorp PJ, Busse R, Brandes RP. Xanthine oxidase inhibitor tungsten prevents the development of atherosclerosis in apoe knockout mice fed a western-type diet. *Free Radical Biology & Medicine.* 2006;41: 1353–1360.

Supplemental Materials and Methods

Reagents

Primary Ab for western blotting were purchased from Santa Cruz: anti-VCAM1 (#sc-8304), anti-ICAM1 (#sc-1511), anti-MCP-1 (#sc-1784), anti-MMP2 (#sc-10736) and anti-MMP9 (#sc-6840).

Assay of phagocytic activity

The indicated concentration of allopurinol was added to the medium 2h prior to additional incubation with 10ng/ml LPS or 1% WHHL rabbit serum for 24h. The phagocytic activity of J774.1 cells, treated as described above, was assayed using a phagocytosis assay kit (IgG FITC, Cayman Chemicals) according to the manufacturer's instructions. In brief, latex beads coated with fluorescently-labeled rabbit-IgG served as a probe for quantification of the phagocytic process *in vitro*. The engulfed fluorescent-beads were detectable using a Leica DMIRB microscope, with excitation and emission at 485 and 535 nm.

Supplemental Figure Legends

Supplemental Figure I

XOR expression. a. XOR expression in the aortic root. Macrophages and XOR

expression were visualized as green and red, respectively. b. Magnified view within the gray square in supplemental figure Ia.

Supplemental Figure II

The phagocytic capability of J774.1 cells was accelerated by stimulation with 1% WHHL serum or 10ng/ml LPS, but neither effect was diminished by allopurinol administration

Supplemental Figure III

Quantification of lipoprotein receptors and ABC transporters involved in lipid transport in J774.1 cells incubated with 30μM allopurinol. Western blotting was performed using specific antibodies for lipoprotein receptors and ABCA1 and ABCG1. Representative bands and quantified band intensities are presented as means±SE. * indicates statistical significance at $p<0.05$. Lipoprotein receptors were suppressed, while ABCA1 and G1 were up-regulated, by allopurinol.

Supplemental Figure IV

Allopurinol effects on secretions of inflammatory cytokines from J774.1 cells induced by 1% WHHL rabbit serum and 10ng/ml LPS. 5a-d, incubation with 1% WHHL rabbit serum, 5e-h, incubation with 10ng/ml LPS. IL indicates interleukin, TNF, tumor necrosis factor. Inflammatory cytokines such as IL-1β, IL-6, IL-12 and TNFα, were dose-dependently inhibited by allopurinol when foam cell formation was triggered by

WHHL serum (IVa-d), while secretions of LPS-induced cytokines, other than IL-6 (IVg), were unaffected by allopurinol (IVe, IVf, and IVh).

Supplemental Figure V

Quantification of key cytokines and molecules which can induce cell migration or contribute to the development of unstable plaques. Monocyte chemoattractant protein (MCP)-1, VCAM-1, ICAM-1 and metaloprotenase (MMP)-2, 9 in J774.1 cells were investigated. J774.1 cells were incubated with 1% WHHL serum or 10ng/ml LPS, with 2 hr prior incubation with 30μg/ml allopurinol. Western blotting was performed using specific antibodies for these proteins. Quantified band intensities are presented as means±SE. * indicates statistical significance at $p<0.05$. Incubation with 1% WHHL serum induced VCAM1, MCP-1 and MMP2, but not ICAM1 or MMP9, expression under these conditions. Allopurinol suppressed the inductions and inhibited MMP9. LPS induced MCP-1 and MMP2, and these inductions were slightly blunted by allopurinol. VCAM1 and MMP9 were suppressed by 10ng/ml LPS, and addition of allopurinol further suppressed both.

Supplement material

Supplemental Figure I

a. b.